Femtosecond hot-exciton emission in a ladder-type π-conjugated rigid-polymer nanowire

D. C. Dai[*] and A. P. Monkman

Department of Physics, Durham University, South Road, Durham DH1 3LE, United Kingdom
(Received 28 November 2011; revised manuscript received 30 June 2012; published 11 January 2013)

A hot exciton is usually the initial elementary excitation product of the solid phase, particularly in low-dimensional photonic materials, which is a bottleneck to all subsequent processes. Measurement of hot-exciton emission (HExEm) is a great challenge due to fast E_K relaxation and thus very weak transient emission. Here, we report the unambiguous observation of femtosecond HExEm from thin films of a model *quasi*-one-dimensional π-conjugated organic rigid-rod quantum nanowire, methyl-substituted ladder-type poly(*para*-phenylenes), using femtosecond time-resolved fluorescence spectroscopy. The results show clear HExEm from the cooling hot excitons, having a lifetime of $\sim$500 to $\sim$800 fs, and concomitant very weak density-dependent singlet-singlet annihilation (SSA) due to this ultrashort dwell time. The ultrafast dispersive migration of the relaxing excitons toward the bottom of the density of states occurs immediately after HExEm, which is simultaneous to the strong density-dependent SSA effect enhanced by the lengthening dwell time.

I. INTRODUCTION

Excitons are the elementary excitation in the solid phase and the primary electronic excited state in low-dimensional photonic materials for (organic) light-emitting device, microcavity laser and photovoltaics, etc., such as polymer, nanotube, C_{60} and graphene, quantum well, wire, and dot.[1–6] Compared to the molecular (Frenkel) and crystalline (Wannier-Mott) excitons, *quasi*-one-dimensional (1D) excitons are of intermediate form, which is always bound to a wire, but may develop across two wires. The strong quantum confinement effect and electron-phonon coupling stabilize these excitons so that they are dominant from low to high temperatures.[1–6]

A hot exciton[7] is usually the initial excitation product caused by photogeneration or charge recombination, for example, it is considered as an exciton with kinetic energy E_K that considerably exceeds the mean thermal energy $k_B T_L$, i.e., $E_K > k_B T_L$, where k_B is the Boltzmann constant and T_L refers to the lattice temperature of the solid.

The current picture of hot-exciton evolution immediately after creation is a very fast E_K relaxation via internal-conversion (cooling),[6,8] and subsequent processes, such as excitation energy transfer (ET), migration and trapping, annihilation, dissociation into polaron pairs or charge-separated states, intersystem crossing of singlet to triplet, formation of biexciton, electron-hole plasma, and Bose-Einstein condensate. Finally, luminescence is given from recombination of the relaxed (cooled) excitons sitting on the lowest-energy states at the bottom of the density of states (DOS), as illustrated in Fig. 1. All of these processes are determined by the basic properties of materials used.[1–6,8] Thus, the hot exciton is a bottleneck for the divergent consequences of exciton evolution; therefore, the investigation of hot excitons has great fundamental importance.

Hot-exciton emission (HExEm), arising from the radiative recombination of hot excitons, is a transient phenomenon, it gives the most direct information on E_K distribution and evolution.[7,8] Since a hot exciton is a thermal nonequilibrium state of the system, the measurement of HExEm is a great experimental challenge due to very fast cooling, i.e., a hot exciton always tends to cool rapidly by emission of

optical and acoustic phonons toward the (*quasi*-) equilibrium state with lower energy. Little direct observation has been convincingly made because of this, and all of the previous reports have been made in the frequency domain[9–16] or are masked by resonant Raman scattering (RRS).[7,8,17] The very recent reports show that tailored HExEm[18,19] is still in the frequency domain and uses a very strong quantum confinement effect in combination with a cavity effect. However, identification of HExEm in the time domain has never been reported. Here, we report the unambiguous femtosecond HExEm from a model π-conjugated rigid-rod organic *quasi*-1D quantum nanowire, methyl-substituted ladder-type poly(*para*-phenylenes) (MeLPPP), using femtosecond time-resolved fluorescence upconversion spectroscopy.

The evolution of excitons in polymers has attracted extensive studies using time-resolved fluorescence spectroscopy in combination with steady-state spectroscopy, and to date, two regimes have been investigated: (i) the dephasing and migration of coherent excitons on femtosecond timescale, for example, a dephasing time $T_2^* = \sim$250 fs has been recently described in nonrigid poly(*para*-phenylene vinylene);[20,21] (ii) all other studies are mainly focused on the spectral shift of luminescence λ_{em} from the migrating relaxed excitons on the picosecond to nanosecond timescale.[22–33] Obviously, there is a clear gap between (i) and (ii): in the frequency domain, this gap appears as a large shift from the excitation λ_{ex} to the onset of λ_{em}, as shown in Fig. 1, which corresponds to initial hot-exciton cooling.[6] If excitation occurs yielding a large E_K, any resultant emission from the hot excitons will lie underneath the strong linear absorption band; therefore, its intensity will be very weak, and it is usually not expected to be observed in experiment.[1–8,20–33] In the time domain, this gap represents a period between T_2^* and $\sim$3 ps. To date, no one has explored the physical processes of hot excitons in π-conjugated polymers because of this.[1–6,20–33]

Femtosecond pump-probe techniques are of little use here due to the superposition of stimulated emission from the hot exciton with photoinduced absorption to high-lying excited states;[2–5,23,34–39] there are also limitations on the availability of the deep-blue spectral component from the white-light supercontinuum needed as a probe.[34–39]
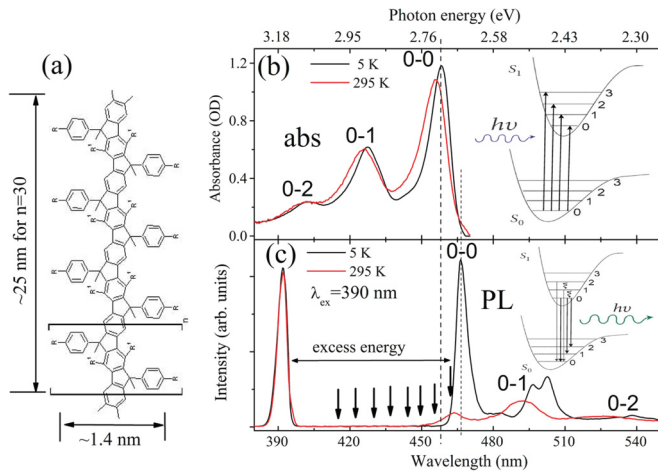
FIG. 1. (Color online) Chemical structure of a rigid-rod MeLPPP nanowire (a), absorption (b), and PL (c) spectra of thin film, R-$C_{10}H_{21}$, and R^1-C_6H_{13}. The downward arrows in (c) indicate the emission wavelengths (λ) monitored. The insets in (b) and (c) show the illustrating potential diagrams of energy levels and the corresponding optical transitions.

In pristine thin films, π-conjugated polymers are typically amorphous glasses, having a statistical distribution of chain lengths and random orientations, and each chain usually is composed of multiple segments due to chain folding, twisting, kinks, or chain defects, etc., and all of these yield poorly resolved absorption and emission spectra and provide a large heat bath to enable excitons to migrate nondispersively over relatively large distance during their lifetimes.[1–6,20–39] Moreover, the rich vibronic modes and the strong electron-phonon coupling on each single chain greatly broaden the overall optical transition cross sections in absorption and emission.[1–6,20–39] These all conspire to produce large degrees of homogenous and inhomogeneous broadening with concomitant very short T_2 and T_2^*, respectively, usually on the scale of a few hundred femtoseconds or less,[20,21] whereas ladder-type poly(*para*-phenylene) is a class of rigid-rod *quasi*-1D organic quantum wire with discrete chain sizes,[40] as a result of inter-repeat unit methylene bridges [see Fig. 1(a) for structure]. They can be easily synthesized at high purity (>99%) and low polydispersity (PD) of chain length. All of these features have lead to the observation of nearly perfect symmetric spectral line shapes in molecular spectroscopy,[40,41] which is shown in Fig. 1, and the estimated longest $T_2^* = $ ∼520 fs for a single chain at low temperature.[42] Therefore, MeLPPP is an ideal model representing polymer chains and rigid inorganic nanowires, for investigation of exciton dynamics.

II. EXPERIMENTAL METHODS

The pristine films of MeLPPP (purity > 99.5%, $M_n = $ 25 kDa, approximately $n = 30$, PD 1.3) were made by spin coating onto sapphire substrates from toluene solution, 15 mg/ml. The typical thickness is ∼125 nm. Samples are mounted in a helium closed-cycle cryostat for both 5.0 K and room-temperature measurements. The cryostat is mounted on

a manual yz stage, which allows continuous movement of laser spot on the sample without altering the optical path and shifting the time delay in the femtosecond experiment.

The chemical structure of a single MeLPPP nanowire, optical absorption, and photoluminescence (PL) spectra of MeLPPP film are shown in Fig. 1. A fiber-coupled charge-coupled device spectrometer (Ocean Optics USB 4000) is used to monitor the backward emission from the film, and record PL and absorption spectra, in the latter case in combination with a tungsten lamp. The PL quantum yields estimated at very low excitation power (P) are ∼50% and ∼25% at 5 K and room temperature, respectively, which are consistent with previous reports.[43,44]

The experimental setup of femtosecond time-resolved fluorescence upconversion spectroscopy has been used in our previous work,[45] which is similar to others in reports.[22–28,30–32] The laser source is a commercial $\tau_p = 180$ fs amplifier system (Coherent RegA 9000), which delivers 5.0-μJ pulses at 100 KHz and 780 nm (1.59 eV). The second harmonic pump beam at 390 nm (3.18 eV), with a pulse duration $\tau_{ex} = $∼280 fs, is focused by a singlet lens to a round spot with a diameter of 100 μm on the MeLPPP films at an incident angle of ∼3°. The forward emission is collected by another singlet lens and converged onto a 0.50 mm beta-barium borate crystal, in which the fluorescence is upconverted by a gating beam at 780 nm. The upconversion beam passes through a double monochromator (JY Gemini) and reaches the detector, a photon-counting solar-blind photomultiplier tube (PMT). The signal intensity from the PMT is recorded by a gated photon-counting technique with respect to the time delay between pump and gating pulses (Becker & Hickl PMS 400A). The typical response time of the system is $\Delta t = 360$ fs, as will be shown in Figs. 2(b) and 4(a) as the t_0 pulse, which is the cross correlation of pump scattering and gating beam. The
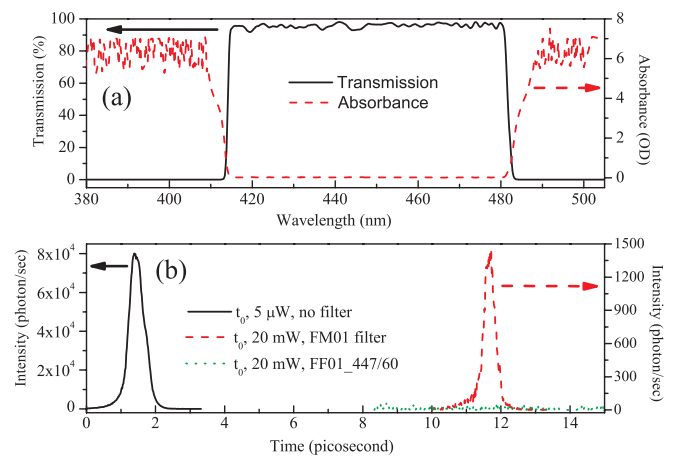
FIG. 2. (Color online) Blocking efficiency of excitation scattering by the filter FF01_447/60. (a) Transmission and absorbance spectra of the filter, showing an effective transmission window between 413 and 482 nm. (b) Comparison of t_0 pulses recorded as the system response function, showing the excitation scattering (max. 8×10^4 at $P = 5$ μW) can be efficiently attenuated by the filter FM01 (max. 1400 at 20 mW), and completely blocked by FF01 (0 at 20 mW). The time delay of t_0 pulse is induced by the thickness of filter; both filters have similar thickness in millimeters.
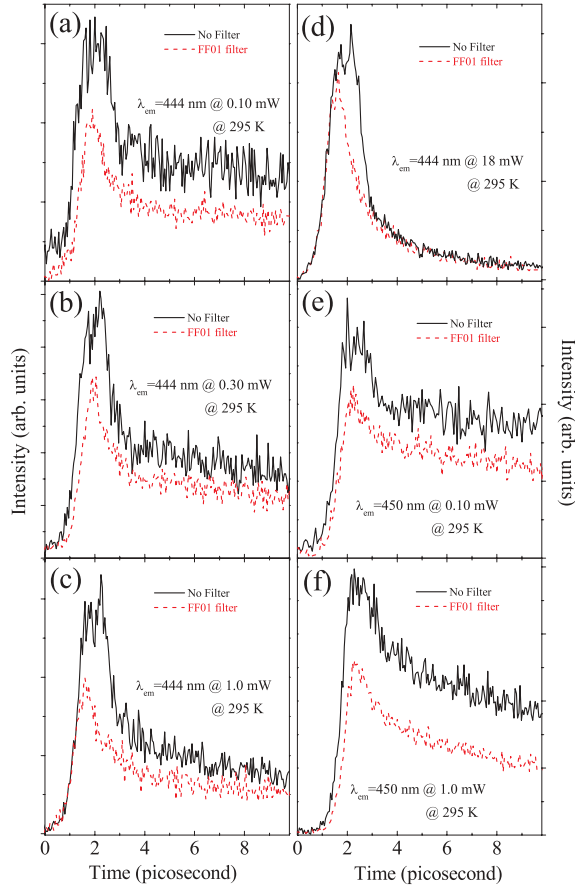
FIG. 3. (Color online) Comparison of experimental data with and without the filter FF01. (a)–(f) Showing apparent distortions within the first few picoseconds induced by excitation scattering.

FIG. 4. (Color online) wavelength-(λ) dependent ultrafast emission dynamics of the hot and cooled excitons in MeLPPP at 5 K. t_0 pulse is shown for clear comparison.

spectral response bandwidth measured is $\sim$3 nm. The pump power (P) is varied with a neutral density filter wheel, $P = 1.0$ mW, which means that a single pulse has energy of 10 nJ or 2.0×10^{10} photons; the corresponding pump influence and transient power density are 127 μJ cm^{-2} and 0.637 GW cm^{-2}, respectively; other values of P have a simple linearity to this. A bandpass filter (FF01_447/60, Semrock) is used to fully block the excitation scattering at $\lambda_{ex} = 390$ nm, which usually distorts the signals in the first few picoseconds. The test results for t_0 pulse and signal trace are shown in Figs. 2 and 3, respectively, comparing another filter, FM01 (Thorlabs Inc.); these ensure full validity of the data in the first few picoseconds.

III. EXPERIMENTAL RESULTS

The spectra in Fig. 1, with a very small Stokes shift indicative of a true rigid-rod chain,[40] represent Franck-Condon transitions for excitonic states in MeLPPP. The excitation laser directly creates a hot-exciton population N_λ in the first electronic excited state manifold $S_1 v_{2,j}$, (j signifies a low-energy chain-breathing mode[41] of $\sim$14 meV) with an excess energy of $\sim$0.47 eV with respect to the 0-0

absorption maximum ($S_0 v_0 \rightarrow S_1 v_0$) at $\sim$457 nm (2.71 eV). This is at least twice the energy of C $=$ C vibronic modes ($\sim$1600 cm$^{-1} \cong 0.20$ eV).[41] Here N_λ is proportional to P.

In a sketch view, Fig. 4 depicts the wavelength-(λ) dependent ultrafast dynamics of exciton emission in MeLPPP film at 5 K at $P = 0.30$ mW. The full details recorded are plotted in Fig. 5. The fitting results by exponential functions are summarized in the Appendix. The emission at $\lambda = 437$ nm (2.84 eV), 444 nm (2.79 eV), and 449 nm (2.76 eV) in Figs. 4 and 5(a)–5(c) all exhibit weak but clear peaks, which cannot be observed from a bare sapphire substrate only. These lie deep beneath the absorption band and correspond to the radiative transition $S_1 v_{1,j} \rightarrow S_0 v_0$ and are therefore interpreted to be HExEm from the cooling hot exciton. Their emission profiles are all similarly pulselike and have a clear average time delay $\tau_d \cong 0.32$ ps with respect to t_0 [shown in Fig. 5(a)]. This τ_d marks a period of initial T_2^* process and internal conversion from $S_1 v_{2,j}$ to $S_1 v_{1,j}$. These pulse widths [full width at half maximum, (FWHM)] are all typical: $\tau_W = 1.0 \pm 0.10$ ps at $P = 0.30$ mW, slightly shortens to 0.80 ± 0.10 ps at 10 mW for both 437 and 444 nm, and 1.0 ± 0.10 ps at 449 nm. These values are appreciably longer than the width of t_0, $\Delta t = 360$ fs, indicating that the time resolution of our system is sufficiently short to resolve these ultrashort emission features. The pulselike peaks of HExEm shown in Figs. 4 and 5(a)–5(c) are on a logarithmic intensity scale, except for Fig. 5(a), and are cross-correlation traces between the real HExEm (duration τ_{HExEm}) and the upconversion gating pulse ($\tau_p = \sim$180 fs). Therefore, τ_{HExEm} can be calculated by ($\tau_W - \tau_p$), thus $\tau_{HExEm} \cong 500$ fs to $\sim$800 fs is appreciably longer than the $\tau_{ex} = \sim$280 fs. As the observation window moves from 437 to 449 nm, the decays become more developed with well-resolved trailing edges, and all show an excellent fit to a single exponential function: the lifetimes at $\lambda = 437$ and 444 nm are from $\tau = 0.60 \pm 0.05$ ps at $P = 0.30$ mW to 0.50 ± 0.05 ps at 10 mW, whereas at $\lambda = 449$ nm, τ is slightly longer, from 0.85 ± 0.05 ps at 0.30 mW to 0.75 ± 0.05 ps
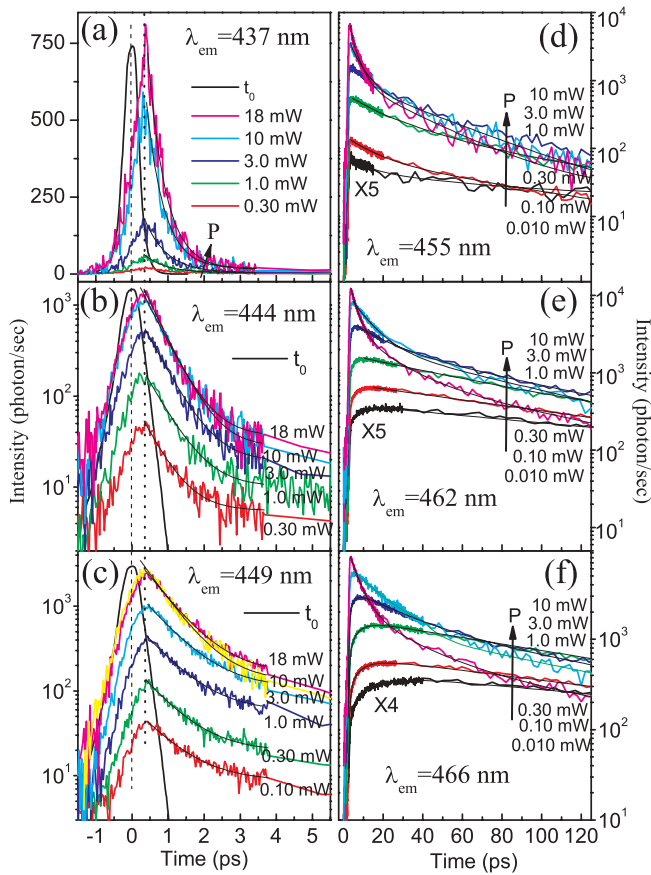
FIG. 5. (Color online) Excitation power (P) and wavelength-(λ) dependent ultrafast emission dynamics of the hot and cooled excitons in MeLPPP at 5 K. The thin line on each curve is the exponential fitting, and the arrows with P indicate the increase of excitation power; these apply to the subsequent figures.

at 10 mW. This is attributed to the contribution of HExEm from the excitons on the upper $S_1 v_{0,j}$ states. At each λ, the values of τ_W and τ at high P are slightly shorter than low P. This is attributed to the very weak excitonic singlet-singlet annihilation (SSA) effect, which slightly decrease the exciton density N_λ, thus τ as P increases.

At $\lambda = 455$ nm (2.73 eV), we are nearly at the 0-0 absorption maximum at $\sim$457 nm, and the onset of λ_{em} (Fig. 1) E_K is rather small; thus, HExEm is not expected. The emission dynamics in Figs. 4 and 5(d) show clearly different behaviors from the previous λ: the curve at low P (<0.30 mW) fits well to a biexponential decay, a fast $\tau_2 = 10 \pm 1$ ps, and a slow $\tau_1 = 75 \pm 5$ ps. These emergent very long lifetimes are indicative of emission from the fully cooled excitons N_λ migrating toward the bottom of the DOS. At moderate P (0.30 mW $< P <$ 3.0 mW), there are the clear first signs of fluorescence lifetime quenching due to the onset of SSA on increased N_λ. At $P > 3.0$ mW, a very fast lifetime $\tau_3 = 0.70 \pm 0.05$ ps appears, indicating the growing efficiency of SSA, which effectively outcompetes all other decay channels at very high N_λ. This should not be confused with the previous HExEm from the cooling hot excitons. These results show that the excitons N_λ become "trapped" on these relatively

high-energy chains and the SSA becomes effective with the enormously increased dwell time τ of the excitons on these chains.

At $\lambda = 462$ nm (2.68 eV), with the blue edge of the $S_1 v_{0,j} \rightarrow S_0 v_0$ emission band (Fig. 1), the possibility of HExEm can be completely ruled out, and a clear build-in is observed immediately after t_0 [see Fig. 5(e)], indicating the cooled excitons N_λ migrating into this detection window. A single exponential growth fit gives a build-in time from $\tau_{gr} = 9.0 \pm 1$ ps at $P = 0.010$ mW to 5.0 ± 0.5 ps at 0.30 mW, in agreement with the fast decay τ_2 at 455 nm, and indicative of increasing migration-induced filling of lower-energy (DOS) states. Above 1.0 mW, SSA tends to dominate the decays, and build-in disappears. At low N_λ, the decay is also typical of a single exponential, giving a $\tau_1 = 160 \pm 10$ ps at 0.010 mW. Some quenching to 120 ± 10 ps at 0.10 and 0.30 mW due to the weak SSA is seen. As $P > 0.30$ mW, a $\tau_2 = 31 \pm 10$ ps can be resolved and shortens to 7.0 ± 1 ps as $P > 1.0$ mW, also consistent with τ_2 at 455 nm. Again at high P (>10 mW), an ultrashort $\tau_3 = 1.0 \pm 0.1$ ps emerges, indicative of efficient SSA not HExEm.

At $\lambda = 466$ nm (2.66 eV), with the onset of absorption and the peak of the $S_1 v_{0,j} \rightarrow S_0 v_0$ transition, the emission emanates primarily from the fully cooled and immobilized excitons N_λ that have migrated to the bottom of the DOS. Concomitant with this, a long population accumulation (build-in) process spans >30 ps at $P = 0.010$ mW, having an exponential growth of $\tau_{gr} = 12 \pm 2$ ps, which gradually shortens to 3.0 ps at 1.0 mW [Fig. 5(f)] due to the increasing filling rate at high N_λ. As $P > 3.0$ mW, the build-in disappears due to SSA again. The single exponential decays at 0.010 and 0.10 mW give $\tau_1 = 200 \pm 10$ ps and 180 ± 10 ps, respectively, representing the longest fluorescence lifetime measurable. At 0.30 mW the curve turns biexponential, indicative of very slow migration further down the DOS at high N_λ again. At 10 mW, again SSA starts to dominate, giving $\tau_3 = 1.0 \pm 0.1$ ps; this is all consistent with 462 and 455 nm.

In contrast to 5 K, given $k_B T_L \cong 26$ meV at room temperature, there is a large amount of thermally activated vibronic and chain-breathing modes in MeLPPP, and hence a faster T_2^* and broadened E_K distribution.[7,41] The spectral peaks and onset of λ_{em} all undergo blueshift; the PL quantum yield is greatly reduced to $\sim$25%, particularly, the 0-0 emission is much weaker than the 0-1 emission primarily due to self-absorption (Fig. 1). These results are detailed in Figs. 6 and 7.

The weaker but still clear HExEm at $\lambda = 415$ nm (2.99 eV), 422 nm (2.94 eV), and 430 nm (2.88 eV) all have similar pulse widths, $\tau_W \cong 0.80$ ps (0.70–0.90 ps), and the same decays, $\tau = 0.45 \pm 0.05$ ps [Figs. 6(a)–6(c)]. Within experimental uncertainty, these are the same as at 5 K. At 437 nm (2.84 eV), τ_W lengthens to 1.0 ± 0.10 ps, and the lifetime to $\tau = 0.60$ to 0.80 ± 0.05 ps [Fig. 6(d)], indicating a slight slowing down of hot-exciton cooling than previous λ, again in line with what we see at the 5-K prefluorescence onset.

The blueshift of the onset of λ_{em} to 444 nm (2.79 eV) is further indicated by biexponential decays in Fig. 6(e): a slow $\tau_1 = 50 \pm 10$ ps indicates some cooled excitons dwelling on these sites and a fast $\tau_3 = 1.0 \pm 0.10$ ps sitting on the slow component, which is independent of P and is consistent with $\lambda = 437$ nm in Fig. 6(d), is clearly HExEm.
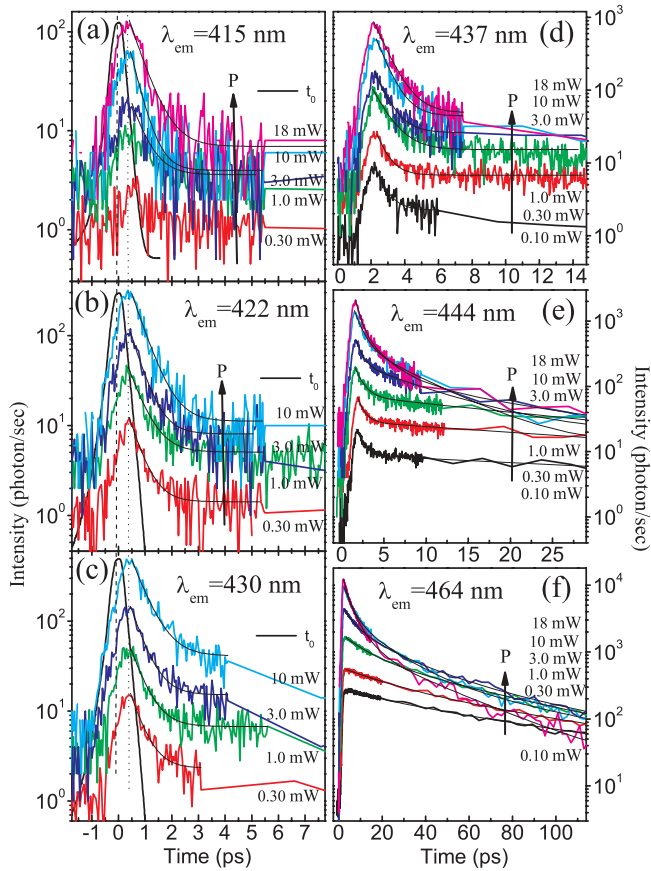
FIG. 6. (Color online) P-dependent ultrafast emission dynamics of the hot and cooled excitons in MeLPPP at room temperature.
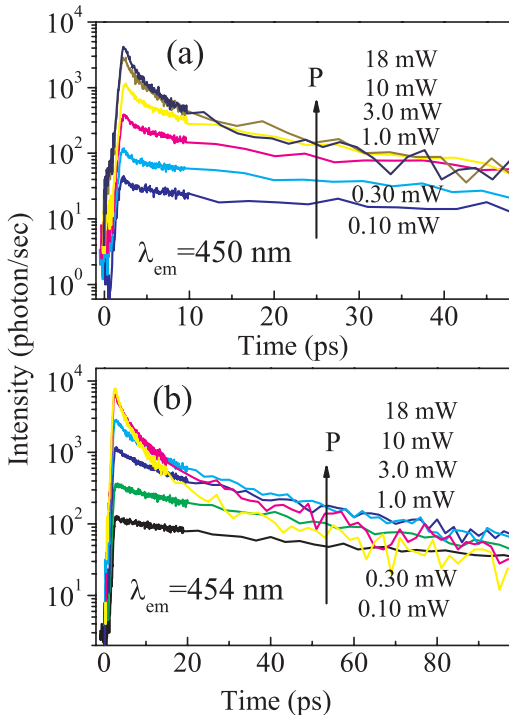
FIG. 7. (Color online) P-dependent ultrafast emission dynamics of migrating excitons in MeLPPP at room temperature.

At longer λ, the data are shown in Fig. 7, the HExEm disappears, and the migration component is seen again. At 464 nm (2.67 eV) in Fig. 6(f), the 0-0 emission peak, a slow $\tau_1 = 85 \pm 10$ ps at 0.10 and 0.30 mW, shortens to 60 ps at 10 mW. This is much shorter than $\tau_1 = 200$ ps at 5 K and is ascribed to thermally enhanced quenching, which also causes the large reduction on PL quantum yield. A fast $\tau_2 = 20 \pm 5$ ps at 0.10 mW and 15 ps at 10 mW indicates the excitons are still actively migrating to lower-energy states in the DOS, but the slow build-ins are not observed, indicative of being at thermal equilibrium and thus nondispersive migration. A $\tau_3 = 9.0 \pm 1.0$ ps emerges at 1.0 mW and shortens to ~ 3.0 ps as $P > 10$ mW, resulting from SSA effect, which is enhanced by thermally activated hopping.

IV. DISCUSSIONS

A. HExEm is from incoherent hot excitons

The excitation pulse ($\lambda_{ex} = 390$ nm and $\tau_{ex} = \sim 280$ fs) initially created coherent hot excitons N_λ become incoherent rapidly within the dephasing time $T_2^* = \sim 520$ fs[42] most probably by the emission of lower-energy phonons than the chain-breathing mode at 113 cm^{-1} (14 meV),[41] which has a vibrational period of 295 fs and very possibly corresponding to the observed $\tau_d = \sim 0.32$ ps. Given that the wavelengths of HExEm are all apparently longer than $\lambda_{ex} = 390$ nm, we conclude that the observed HExEm is from the incoherent and cooling hot exciton. The possible distortion by excitation laser has been totally ruled out with the use of the bandpass filter FF01, which has been discussed in Sec. II.

B. Exclusion of ET within oligomers and short-chain segments

The PD of the MeLPPP used in these measurements is 1.3, purity > 99.5%, $M_n = 25$ kDa, approximately $n = 30$. All short-chain oligomers are removed by multiple column purification with good solvent. The PD is indicative of the polymer with no chains shorter than 20 repeat units. This is confirmed by the sharpness of the absorption spectra resolution in Fig. 1(b).

Further, the HExEm emanating at $\lambda < 437$ nm cannot be from any residual short-chain oligomers or short-chain segments, given that (i) the emission peak of an $n = 11$ chain is observed at 449 nm and a pentamer ($n = 5$) at 437 nm.[46–48] (ii) The femtosecond decay times cannot be explained by Forster-Dexter ET induced quenching effects:[49,50] the estimated ET efficiency needed to obtain such rapid transfer, $E = \sim 99.6\%$ is far too high, and the estimated separation distance $r \cong 2.0$ nm is much smaller than the minimum chain separation due to the side-chain spacing effect. Further details are given in the following Secs. IV F and IV G.

C. Exclusion of RRS

HExEm is easy to confuse with RRS at time t_0.[7,8,17] Here, RRS can be completely ruled out as it cannot explain any of the observed features: the $\tau_d \cong 0.32$ ps, the broader $\tau_W = \sim 0.80$ ps than the $\tau_{ex} = \sim 280$ fs and $\Delta t = 360$ fs,

the gradually increasing emission intensity and lengthening decays with increasing λ at a fixed P, the small nonlinear amplitude increase with increasing P, and the temperature effect. Thus, we conclude the unambiguous observation of femtosecond HExEm from MeLPPP nanowire. It is not possible to resolve which vibronic modes contribute to the HExEm as the vibronic manifold is complex with many overtones from low-energy modes.[41,51] Whereas the weak HExEm suggests a tiny fraction of N_λ on the $S_1 v_{1,j}$ states recombine directly, the bulk relaxes to the $S_1 v_{0,j}$ states during the first ~ 1.0 ps immediately after t_0.

D. Dispersive exciton migration

From our data, the exciton migration clearly takes place immediately after the hot-exciton cooling and depends on N_λ, λ, and $k_B T_L$. The increasing decays (τ_1 and τ_2) with λ is a clear indication of dispersive singlet exciton migration,[3,22–39] confirmed by the increasing τ_{gr} with λ at 5 K. $k_B T_L = \sim 26$ meV at room temperature straightforwardly means a significant Boltzmann population in the low-energy phonon modes; hence, the migration starts at shorter λ, and we do not observe the build-in of λ_{em} as at 5 K.

E. Exciton annihilation effect

Our results also indicate that the SSA is determined by exciton density N_λ,[3,39] which is equivalent to an average exciton-exciton separation, and is more sensitive to $k_B T_L$ and the dwell time τ on the sites at λ. This allows excitons to find quenching sites throughout the film, thus explaining the much lower PL quantum yield at room temperature than at 5 K and the very weak SSA in HExEm.

F. Estimation of Forster resonance energy transfer efficiency (E) and rate (k_{ET})[49,50]

The measured quantum yield $Q_0 \cong 25\%$ at 295 K for MeLPPP thin film is consistent with previous literature reports.[43,44] By comparing the integrated area of the PL spectra in Fig. 1(c), we obtain $Q_0 \cong 50\%$ at 5 K.

Fitting the decay curve for $\lambda_{em} = 466$ nm at low P in Fig. 5(f) gives $\tau_0 = 200$ ps, then $\tau_{rad} = \tau_0/Q_0 = 400$ ps. At $\lambda_{em} = 466$ nm, ET does not takes place given it is the bottom of the DOS, so it has no overlap integral; thus, the decay rate

$$k_{rad\_466\,nm} = (k_f + \Sigma k_i) = \frac{1}{\tau_{rad}} = \frac{1}{400\ \text{ps}} = 2.5 \times 10^9\ \text{sec}^{-1}.$$

Here, k_f is the fluorescence decay rate, k_i are the rate constants of any other de-excitation pathway, including annihilation.

Suppose some segments existing in MeLPPP film give emission at $\lambda_{em} = 442$ nm at 5 K, and we can reasonably assume its $\tau_{rad} = 400$ ps, and $\tau_0 = 200$ ps. With the 0.80 ps in

Fig. 4(b), the Forster resonance energy transfer efficiency,

$$E = 1 - \tau/\tau_{rad} = 1 - 0.80/400 = 99.8\%.$$

Obviously, this value is too high to be physical.[49,50] With this value, a ten-step ET will have a final efficiency, $E = (99.8\%)^{10} = 96.0\%$. If this were true in such an amorphous polymer film, it is totally comparable to the photosynthetic system, where the proteins have clear stereo chemical configurational and conformational structures than the amorphous film used here, and in a common belief its $E = \sim 95\%$ is within several steps. However, to date, the real ET mechanism in the photosynthetic system has not been well understood.[52]

Accordingly, if the decay rate at $\lambda_{em} = 442$ nm does include a contribution from ET, then

$$k_{rad-442\,nm} = k_{ET} + (k_f + \Sigma k_i) = \frac{1}{\tau} = \frac{1}{0.80\ \text{ps}}$$
$$= 1.25 \times 10^{12}\ \text{sec}^{-1} \approx k_{ET} \gg 2.5 \times 10^9\ \text{sec}^{-1}.$$

Here, the rate $k_{ET} = 1.25 \times 10^{12}$ sec^{-1} would almost be the highest reported in literature, which is not credible.

G. Estimation of Forster ET distance (r)[49,50]

The Forster ET equation is

$$k_{ET} = (k_f + \Sigma k_i)\left(\frac{R_0}{r}\right)^6 = \frac{1}{\tau_{rad}}\left(\frac{R_0}{r}\right)^6.$$

Here, R_0 is the Forster radius at which the ET efficiency is 50%.

Combining the previous k_{ET} value gives

$$k_{ET} = \frac{1}{400\ \text{ps}}\left(\frac{R_0}{r}\right)^6 = 1.25 \times 10^{12}\ \text{sec}^{-1},$$
$$r = 0.355 R_0.$$

For $\tau = 0.40 - 1.0$ ps from HExEm decay in Figs. 4 and 5, correspondingly the range of r would be

$$r = 0.316 R_0 \sim 0.369 R_0.$$

An estimated $R_0 = 5.31$ nm is given in the appendix, which is very large for these systems.[49,50] Thus, this yields $r = \sim 2.00$ nm and is approximately equivalent to two repeat units 1.68 nm, which means that two excitons should be separated by between two and three repeat units on a single chain. However, this separation cannot be an interchain distance given the side group of a MeLPPP chain with ten C-C bonds seriously prohibits such short interchain distances. Moreover,

$r = \sim 2.00$ nm is more indicative of Dexter ET, which is more efficient than Forster ET as the separation is below ~ 2.0 nm. However, we have not seen any previous report using the Dexter ET model to deal with the singlet exciton ET; it is generally used for triplet ET.

For ET to occur over such short distances in such a short timescale, subpicoseconds would imply that the exciton density initially photocreated needs to be many orders of magnitude greater than that used in our experiments and as a consequence completely rules out Dexter ET processes on this initial subpicosecond timescale.

V. CONCLUSIONS

By using femtosecond time-resolved fluorescence spectroscopy in a holistic view, we have clearly observed the unambiguous femtosecond incoherent HExEm from a π-conjugated polymer nanowire, MeLPPP, and the subsequent dispersive exciton migration toward the bottom of the DOS immediately after hot-exciton cooling, and the exciton annihilation is codominated by density and dwell time. We further confirm our previous result that singlet annihilation is controlled by exciton migration. We show that these exciton dynamics are a direct result of the rigid chain structure of the ladder-type polymer that processes weak electron-phonon coupling. This causes slow internal conversion and strong excited state ground-state coupling, which enables radiative decay from the hot states to compete with internal conversion. Further weak electron-phonon coupling also ensures at low temperatures that exciton self-localization is ineffective and nondispersive exciton migration continues throughout the lifetime of the excitons. At room temperature there is a sufficient phonon bath for nondispersive migration to dominate, and so exciton mobility increases, which also increases the probability of SSA.

ACKNOWLEDGMENT

APPENDIX

1. Estimation of R_0[49,50]

The optical density (OD) is defined as $\mathrm{OD} = A = -\log(\frac{I}{I_0}) = \alpha l$.

The Beer-Lambert law is $A' = -\ln(\frac{I}{I_0}) = \alpha' l$.

Thus, $A' = A \ln(10) \approx 2.303 A$ and $\alpha' = \alpha \ln(10) \approx 2.303 \alpha$,

given $\alpha' = \frac{4\pi}{\lambda} k$, where k is the extinction coefficient.

Thus, $k = 0.183 \frac{A}{l} \lambda$.

From the literature,[46–48] for $n = 12$ the MeLPPP oligomer or segment has the 0-0 absorption peak at ~ 442 nm in solution at room temperature, which has a similar shape as in Fig. 1(b); thus, for estimation of R_0 at 5 K, we set both absorption and PL
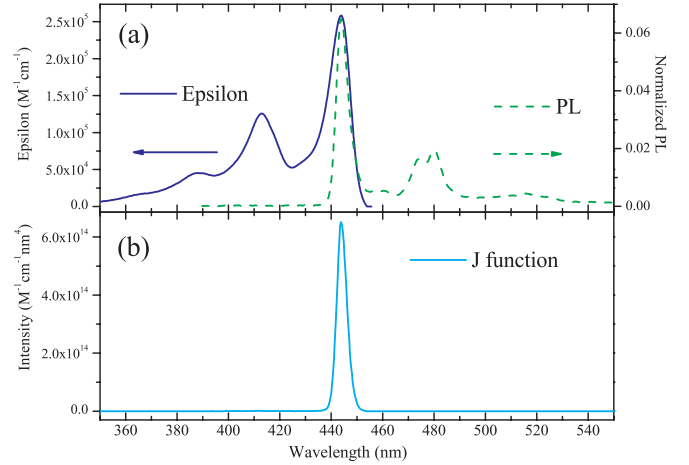
FIG. 8. (Color online) Spectral overlap J function for an estimation of R_0. (a) Spectral overlap. (b) Calculated J function.

0-0 peaks at ~ 442 nm for the best spectral overlap, as shown in Fig. 8.

The normalized PL spectrum is shown in Fig. 8(a).

Using $k = 0.183 \frac{A}{l} \lambda$, $l = \sim 120$ nm (the thickness of MeLPPP thin films in our experiment), A is the measured OD value [shown in Fig. 1(b)], and the absolute extinction coefficient k has a maximum of 0.80 at ~ 442 nm. The reported ε value is 2.58×10^5 M^{-1}cm^{-1} at ~ 442 nm,[47,48] which is used to calibrate the k spectrum, and the resultant ε curve is shown in Fig. 8(a). The calculated spectral overlap is also shown in Fig. 8(b), $J = 3.315 \times 10^{15}$ (M^{-1} cm^{-1}nm^4), this yields

$$R_0^6 = 8.79 \times 10^{-5} [k^2 \eta_D n^{-4} J(\lambda)],$$

with $\eta_D = Q_0 = 50\%$, $k^2 = 2$, the orientation factor, $n = 1.90$, the typical refractive index of MeLPPP film, $R_0^6 = 2.235 \times 10^{10}$; thus, $R_0 = 5.31$ nm, and this is a normal value for Forster radius.[49,50]

Thus, $r = 0.398 R_0 = 2.11$ nm and $r = 0.355$ $R_0 \sim 0.414 R_0 = 1.89$ nm ~ 2.20 nm.

In our estimation $\kappa^2 = 2$ is assumed (normally $0 \leqslant \kappa^2 \leqslant 4$). The ordinary $\kappa^2 = 2/3$ is applicable when both segments are freely rotating and can be considered to be isotropically oriented during the excited state lifetime. If either segment is fixed or not free to rotate, like our case, the fluorescent segments in the pristine thin films of MeLPPP cannot reorient on the femtosecond timescale, which is much faster than the ET time observed in our experiment, then $\kappa^2 = 2/3$ is not a valid assumption; thus, we use $\kappa^2 = 2$. In most cases, even modest reorientation of the segments results in enough orientational averaging that $\kappa^2 = 2/3$ does not result in a large error in the estimated ET distance due to the sixth-power dependence of R_0 on κ^2.[49,50] Even when κ^2 is quite different from $2/3$, the error can be associated with a shift in R_0, and thus determinations of changes in relative distance for a particular system are still valid.[49,50] For example, with $\kappa^2 = 2/3$, similarly, $R_0^6 = 0.745 \times 10^{10}$, $R_0 = 4.42$ nm, and $r = 0.355 R_0 \sim 0.414 R_0 = 1.57$ nm ~ 1.83 nm < 2.0 nm.

The summary of fitting results by exponential growing or decay functions to the data in Figs. 5 and 6.

437 nm, 5 K	0.30 mW	1.0 mW	3.0 mW	10 mW	18 mW
Exp decay	0. 61 ps	0. 59 ps	0. 60 ps	0.48 ps	0.49 ps
FWHM	1.0 ps	0.83 ps	0.90 ps	0.76 ps	0.80 ps

444 nm, 5 K	0.30 mW	1.0 mW	3.0 mW	10 mW	18 mW
Exp decay	0. 54 ps	0. 59 ps	0. 56 ps	0.53 ps	0.51 ps
FWHM	0.95 ps	0.97 ps	0.98 ps	0.80 ps	0.88 ps

449 nm, 5 K	0.10 mW	0.30 mW	1.0 mW	3.0 mW	10 mW	18 mW
Exp decay	0.88 ps	0. 83 ps	0. 85 ps	0. 85 ps	0.77 ps	0.70 ps
FWHM	1.27 ps	1.04 ps	1.14 ps	1.15 ps	1.00 ps	1.00 ps

455 nm, 5 K	0.010 mW	0.10 mW	0.30 mW	1.0 mW	3.0 mW	10 mW	18 mW
Exp decay 1					0.55 ps	0.58 ps	0.55 ps
Exp decay 2	11 ps	13 ps	20 ps	12 ps	5.5 ps	3.9 ps	3.3ps
Exp decay 3	78 ps	78 ps	78 ps	61 ps	47 ps	29 ps	25 ps

462 nm, 5 K	0.010 mW	0.10 mW	0.30 mW	1.0 mW	3.0 mW	10 mW	18 mW
Exp grow 1	1.0 ps	0.73 ps	0.97 ps	0.74 ps	0.76 ps	1.0 ps	1.0 ps
Exp grow 2	8.8 ps	4.2 ps	4.9 ps	3.3 ps			
Exp decay 1			31 ps	7.1 ps	7.9 ps	6.4 ps	12 ps
Exp decay 2	157 ps	121 ps	119 ps	74 ps	44 ps	58 ps	67 ps
Exp decay 3					133 ps		

466 nm, 5 K	0.010 mW	0.10 mW	0.30 mW	1.0 mW	3.0 mW	10 mW	18 mW
Exp grow 1	1.0 ps	1.4 ps	1.0 ps	0.76 ps	0.85 ps	0.84 ps	1.3 ps
Exp grow 2	13.4 ps	11.6 ps	6.8 ps	3.3 ps			
Exp decay 1			64 ps	26 ps	17 ps	6.9 ps	5.7 ps
Exp decay 2	202 ps	183 ps	162 ps	112 ps	92 ps	63 ps	60 ps

415 nm, 295 K	0.30 mW	1.0 mW	3.0 mW	10 mW	18 mW
FWHM	/	/	0.92 ps	0.92 ps	1.0 ps
Exp decay 1	/	/	0.48 ps	0.38 ps	0.52 ps

422 nm, 295 k	0.30 mW	1.0 mW	3.0 mW	10 mW	18 mW
FWHM	0.70 ps	0.87 ps	0.92 ps	0.87 ps	/
Exp decay 1	0.43 ps	0.50 ps	0.43 ps	0.49 ps	/

430 nm, 295 K	0.30 mW	1.0 mW	3.0 mW	10 mW	18 mW
FWHM	0.87 ps	0.92 ps	0.92 ps	0.87 ps	/
EXP decay 1	0.44 ps	0.48 ps	0.46 ps	0.53 ps	/

437 nm, 295 K	0.10 mW	0.30 mW	1.0 mW	3.0 mW	10 mW	18 mW
FWHM	1.0 ps	1.0 ps	1.0 ps	1.0 ps	1.0 ps	1.0 ps
Exp decay 1	0.59 ps	0.60 ps	0.89 ps	0.73 ps	0.70 ps	0.80 ps

444 nm, 295 K	0.10 mW	0.30 mW	1.0 mW	3.0 mW	10 mW	18 mW
Exp decay 1	0.91 ps	0.75 ps	0.91 ps	0.71 ps	0.92 ps	0.70 ps
Exp decay 2	59 ps	38 ps	27 ps	8.54 ps	6.40 ps	4.60 ps

464 nm, 295 K	0.10 mW	0.30 mW	1.0 mW	3.0 mW	10 mW	18 mW
Exp decay 1	/	/	9.3 ps	4.5 ps	3.4 ps	2.8 ps
Exp decay 2	20 ps	22 ps	21 ps	18 ps	15 ps	15 ps
Exp decay 3	86 ps	86 ps	64 ps	62 ps	63 ps	/

*Present address: The Photon Science Institute, The University of Manchester, United Kingdom; dechang.dai@manchester.ac.uk

[1] G. D. Scholes and G. Rumbles, Nat. Mater. **5**, 683 (2006).

[2] T. Virgili, J. Cabanillas-Gonzalez, L. Luer, and G. Lanzani, in *Photophysics of Molecular Materials: From Single Molecules to Single Crystals*, edited by G. Lanzani (Wiley-VCH, Weinheim, Germany 2006), Chap. 10, p. 525.

[3] I. G. Scheblykin, A. Yartsev, T. Pullerits, V. Gulbinas, and V. Sundstrom, J. Phys. Chem. B **111**, 6303 (2007).

[4] Z. V. Vardeny, in *Ultrafast Dynamics and Laser Action of Organic Semiconductors*, edited by Z. V. Vardeny (CRC Press, Florida, 2009).

[5] U. Scherf and D. Neher, in *Polyfluorenes*, edited by U. Scherf and D. Neher (Springer-Verlag, Heidelberg, 2008).

[6] D. M. Basko and E. M. Conwell, Phys. Rev. B **66**, 155210 (2002).

[7] S. Permogorov, Phys. Status Solidi B **68**, 9 (1975).

[8] K. Hannewald, S. Glutsch, and F. Bechstedt, Phys. Rev. Lett. **86**, 2451 (2001).

[9] K. Murayama and M. A. Bosch, Phys. Rev. B **25**, 6542 (1982).

[10] F. Iikawa, T. Ruf, and M. Cardona, Phys. Rev. B **43**, 4849 (1991).

[11] N. Pelekanos, J. Ding, Q. Fu, A. V. Nurmikko, S. M. Durbin, M. Kobayashi, and R. L. Gunshor, Phys. Rev. B **43**, 9354 (1991).

[12] R. P. Stanley, J. Hegarty, R. Fischer, J. Feldmann, E. O. Gobel, R. D. Feldman, and R. F. Austin, Phys. Rev. Lett. **67**, 128 (1991).

[13] D. Some and A. V. Nurmikko, Phys. Rev. B **48**, 4418 (1993).

[14] M. Nakayama, A. Soumura, K. Hamasaki, H. Takeuchi, and H. Nishimura, Phys. Rev. B **55**, 10099 (1997).

[15] I. G. Ivanov, T. Egilsson, A. Henry, B. Monemar, and E. Janzen, Phys. Rev. B **64**, 085203 (2001).

[16] H. Zhao and H. Kalt, Phys. Rev. B **69**, 233305 (2004).

[17] I. A. Buyanova, G. Yu. Rudko, W. M. Chen, K. Kayanuma, A. Murayama, Y. Oka, A. A. Toropov, S. V. Sorokin, and S. V. Ivanov, Phys. Rev. B **71**, 165203 (2005).

[18] Z. C. Dong, X. L. Zhang, H. Y. Gao, Y. Luo, C. Zhang, L. G. Chen, R. Zhang, X. Tao, Y. Zhang, J. L. Yang, and J. G. Hou, Nat. Photonics **4**, 50 (2010).

[19] C.-H. Cho, C. O. Aspetti, M. E. Turk, J. M. Kikkawa, S.-W. Nam, and R. Agarwal, Nat. Mater. **10**, 669 (2011).

[20] E. Collini and G. D. Scholes, Science **323**, 369 (2009).

[21] F. Milota, J. Sperling, V. Szocs, A. Tortschanoff, and H. F. Kauffmann, J. Chem. Phys. **120**, 9870 (2004).

[22] R. Kersting, U. Lemmer, R. F. Mahrt, K. Leo, H. Kurz, H. Bassler, and E. O. Gobel, Phys. Rev. Lett. **70**, 3820 (1993).

[23] R. F. Mahrt, T. Pauck, U. Lemmer, U. Siegner, M. Hopmeier, R. Hennig, H. Bassler, E. O. Gobel, P. H. Bolivar, G. Wegmann, H. Kurz, U. Scherf, and K. Mullen, Phys. Rev. B **54**, 1759 (1996).

[24] R. Kersting, B. Mollay, M. Rusch, J. Wenisch, G. Leising, and H. F. Kauffmann, J. Chem. Phys. **106**, 2850 (1997).

[25] H. Wang and K. S. Wong, Appl. Phys. Lett. **73**, 1637 (1998).

[26] M. Nisoli, S. Stagira, M. Zavelani-Rossi, S. De Silvestri, P. Mataloni, and C. Zenz, Phys. Rev. B **59**, 11328 (1999).

[27] L. M. Herz and R. T. Phillips, Phys. Rev. B **61**, 13691 (2000).

[28] L. M. Herz, C. Silva, R. H. Friend, R. T. Phillips, S. Setayesh, S. Becker, D. Marsitsky, and K. Mullen, Phys. Rev. B **64**, 195203 (2001).

[29] M. Ariu, M. Sims, M. D. Rahn, J. Hill, A. M. Fox, D. G. Lidzey, M. Oda, J. Cabanillas-Gonzalez, and D. D. C. Bradley, Phys. Rev. B **67**, 195333 (2003).

[30] A. L. T. Khan, P. Sreearunothai, L. M. Herz, M. J. Banach, and A. Kohler, Phys. Rev. B **69**, 085201 (2004).

[31] L. M. Herz, C. Silva, A. C. Grimsdale, K. Mullen, and R. T. Phillips, Phys. Rev. B **70**, 165207 (2004).

[32] P. Sreearunothai, A. C. Morteani, I. Avilov, J. Cornil, D. Beljonne, R. H. Friend, R. T. Phillips, C. Silva, and L. M. Herz, Phys. Rev. Lett. **96**, 117403 (2006).

[33] F. B. Dias, K. T. Kamtekar, T. Cazati, G. Williams, M. R. Bryce, and A. P. Monkman, Chem. Phys. Chem. **10**, 2096 (2009).

[34] W. Graupner, G. Leising, G. Lanzani, M. Nisoli, S. De Silvestri, and U. Scherf, Phys. Rev. Lett. **76**, 847 (1996).

[35] A. Dogariu, D. Vacar, and A. J. Heeger, Phys. Rev. B **58**, 10218 (1998).

[36] T. Virgili, D. Marinotto, C. Manzoni, G. Cerullo, and G. Lanzani, Phys. Rev. Lett. **94**, 117402 (2005).

[37] V. Gulbinas, I. Mineviciute, D. Hertel, R. Wellander, A. Yartsev, and V. Sundstrom, J. Chem. Phys. **127**, 144907 (2007).

[38] T. E. Dykstra, E. Hennebicq, D. Beljonne, J. Gierschner, G. Claudio, E. R. Bittner, J. Knoester, and G. D. Scholes, J. Phys. Chem. B **113**, 656 (2009).

[39] S. M. King, D. Dai, C. Rothe, and A. P. Monkman, Phys. Rev. B **76**, 085204 (2007).

[40] U. Scherf, J. Mater. Chem. **9**, 1853 (1999).

[41] E. W. Snedden, R. Thompson, S. Hintshich, and A. P. Monkman, Chem. Phys. Lett. **472**, 80 (2009).

[42] J. G. Muller, U. Lemmer, G. Raschke, M. Anni, U. Scherf, J. M. Lupton, and J. Feldmann, Phys. Rev. Lett. **91**, 267403 (2003).

[43] J. Stampfl, S. Tasch, G. Leising, and U. Scherft, Synth. Met. **71**, 2125 (1995).

[44] G. Grem, C. Paar, J. Stampfl, G. Leising, J. Huber, and U. Scherf, Chem. Mater. **7**, 2 (1995).

[45] D. C. Dai and A. P. Monkman, Phys. Rev. B **84**, 115206 (2011).

[46] F. Schindler, J. Jacob, A. C. Grimsdale, U. Scherf, K. Mullen, J. M. Lupton, and J. Feldmann, Angew. Chem. **117**, 1544 (2005).

[47] J. Grimme, M. Kreyenschmidt, F. Uckert, K. Mullen, and U. Scherf, Adv Mater. **7**, 292 (1995).

[48] J. Grimme and U. Scherf, Chem. Phys. **197**, 2297 (1996).

[49] J. R. Lakowicz, in *Principles of Fluorescence Spectroscopy*, 2nd ed. (Kluwer Academic, New York, 1999), Chap. 13, pp. 367–388.

[50] G. D. Scholes, Annu. Rev. Phys. Chem. **54**, 57 (2003).

[51] D. Somitsch, F. P. Wenzl, J. Kreith, M. Pressl, R. Kaindl, U. Scherf, G. Leising, and P. Knoll, Synth. Met. **138**, 39 (2003).

[52] G. D. Scholes, Nat. Phys. **7**, 448 (2011).